J. Fluid Mech. (2015), *vol.* 779, R3, doi:10.1017/jfm.2015.465

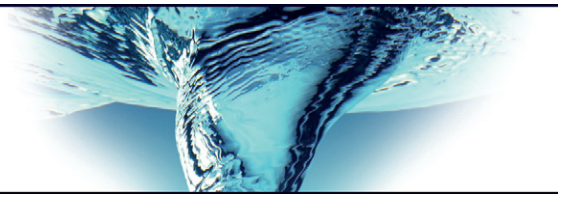

JFM RAPIDS
journals.cambridge.org/rapids

Phase diagram for droplet impact on superheated surfaces

Hendrik J. J. Staat[1], Tuan Tran[2], Bart Geerdink[1], Guillaume Riboux[3], Chao Sun[1,4], José Manuel Gordillo[3] and Detlef Lohse[1,5,†]

[1]Physics of Fluids Group, Faculty of Science and Technology, University of Twente, P.O. Box 217, 7500 AE Enschede, The Netherlands

[2]School of Mechanical and Aerospace Engineering, Nanyang Technological University, 50 Nanyang Avenue, 639798, Singapore

[3]Área de Mecánica de Fluidos, Departamento de Ingeniería Aeroespacial y Mecánica de Fluidos, Universidad de Sevilla, Avenida de los Descubrimientos s/n 41092, Sevilla, Spain

[4]Center for Combustion Energy and Department of Thermal Engineering, Tsinghua University, 100084 Beijing, China

[5]Max Planck Institute for Dynamics and Self-Organization, 37077 Goettingen, Germany

(Received 9 June 2015; revised 31 July 2015; accepted 4 August 2015;
first published online 21 August 2015)

We experimentally determine the phase diagram for impacting ethanol droplets on a smooth, sapphire surface in the parameter space of Weber number *We* versus surface temperature T. We observe two transitions, namely the one towards splashing (disintegration of the droplet) with increasing *We*, and the one towards the Leidenfrost state (no contact between the droplet and the plate due to a lasting vapour film) with increasing T. Consequently, there are four regimes: contact and no splashing (deposition regime), contact and splashing (contact–splash regime), neither contact nor splashing (bounce regime), and finally no contact, but splashing (film–splash regime). While the transition temperature T_L to the Leidenfrost state depends weakly, at most, on *We* in the parameter regime of the present study, the transition Weber number We_C towards splashing shows a strong dependence on T and a discontinuity at T_L. We quantitatively explain the splashing transition for $T < T_L$ by incorporating the temperature dependence of the physical properties in the theory by Riboux & Gordillo (*Phys. Rev. Lett.*, vol. 113(2), 2014, 024507; *J. Fluid Mech.*, vol. 772, 2015, pp. 630–648).

Key words: boiling, drops, drops and bubbles

† Email address for correspondence: d.lohse@utwente.nl

1. Introduction

The transition to splashing, i.e. the disintegration of liquid droplets impacting solid surfaces, has been the subject of numerous studies ever since researchers were able to observe the impact process by high-speed imaging (Worthington 1876; Levin & Hobbs 1971; Rein 1993; Yarin & Weiss 1995; Yarin 2006). Although the splashing mechanism has not been fully understood, it was experimentally found by Xu, Zhang & Nagel (2005) that the pressure of the ambient air is a key factor in the splashing process at room temperature, among others such as the liquid properties (Driscoll, Stevens & Nagel 2010; Palacios *et al.* 2013; Stevens 2014), the droplet's kinetic energy (Yarin & Weiss 1995; Thoroddsen & Sakakibara 1998; Roisman, Rioboo & Tropea 2002; Visser *et al.* 2012, 2015) and the properties of the surface (Mundo, Sommerfeld & Tropea 1995; Lembach *et al.* 2010; Tsai *et al.* 2011; Latka *et al.* 2012; van der Veen *et al.* 2014). In particular, the air layer under the droplet was thought to be responsible for splashing (Mandre, Mani & Brenner 2009; Mani, Mandre & Brenner 2010; Mandre & Brenner 2011; Bouwhuis *et al.* 2012; Kolinski *et al.* 2012), but more recently it was suggested that rather than the gas under the whole droplet, the gas at the edge of the lamella plays a role in the transition to splashing (Riboux & Gordillo 2014, 2015), finding good agreement with the experimental data for isothermal impact at room temperature.

Another transition that has received much attention is the dynamic Leidenfrost transition for droplets impacting heated surfaces (Inada *et al.* 1988; Yao & Cai 1988; Chandra & Avedisian 1991; Bernardin, Stebbins & Mudawar 1997; Wang, Lin & Chen 2000; Sinha-Ray, Zhang & Yarin 2011; Weickgenannt *et al.* 2011; Tran *et al.* 2012, 2013; Quéré 2013; Nair *et al.* 2014; Khavari *et al.* 2015; Shirota *et al.* 2015). When impacting a heated surface, the droplet either makes contact with the surface and boils violently or it is separated from the substrate by a layer of its own vapour for the entire duration of the impact process, the latter being the Leidenfrost state. The lowest surface temperature for which this lasting vapour layer exists is defined as the dynamic Leidenfrost temperature (Tran *et al.* 2012).

What both the transition to splashing and the Leidenfrost transition have in common is that the role of the gas phase between the droplet and the substrate is very relevant. Additionally, both transitions are crucially important in numerous technological and industrial applications; so it is of fundamental and also of practical interest to understand how the transition to splashing depends on the surface temperature and the kinetic energy of the droplet.

The experimental determination of the transition to the Leidenfrost regime is particularly challenging. The distinction of droplet behaviour across the transition has normally relied on high-speed recording of the impact from side or top-angle views. In particular, the appearance of ejected droplets has been used as a criterion by many authors (Inada *et al.* 1988; Yao & Cai 1988; Chandra & Avedisian 1991; Bernardin *et al.* 1997; Wang *et al.* 2000; Tran *et al.* 2012, 2013; Nair *et al.* 2014) to exclude the Leidenfrost state, with the assumption that then there must exist a liquid/surface contact, leading to the disintegration of the droplet. Conversely, it is assumed that a droplet is in the Leidenfrost state when there are no signs of boiling (e.g. vapour bubbles or ejected droplets). However, it is not necessarily true that any liquid/solid contact during impact must produce vapour bubbles or ejected droplets, so this way of classifying impact behaviour might be unreliable. As the existence of a complete vapour layer between the impacting droplet and the solid surface demarcates the

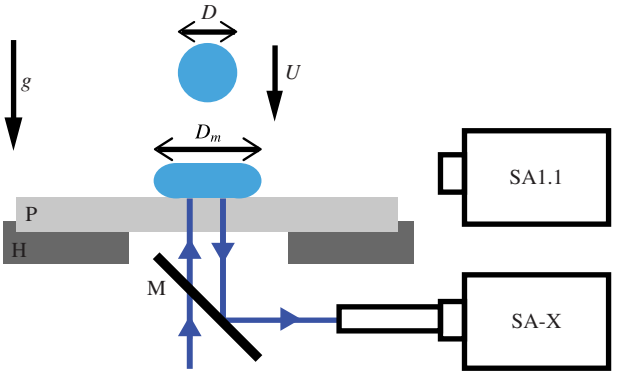

FIGURE 1. Schematics of the experimental set-up, where a droplet of diameter D falls with velocity U on a sapphire plate P, which is placed on a temperature-controlled brass holder H. The impact is recorded by synchronized high-speed cameras from the side (SA1.1) and from the bottom (SA-X). Interferometric bottom-view recording of the impact is achieved by laser illumination from the bottom and a half-mirror M.

Leidenfrost regime from the contact boiling or transition regimes (Khavari *et al.* 2015; Shirota *et al.* 2015), the most accurate means of determining the transition temperature is to measure the vapour layer directly.

In this paper, we present a method based on interferometric high-speed imaging to quantify the Leidenfrost transition temperature in a wide parameter regime. We explore the behaviour of droplets impacting heated surfaces across different regimes separated by the transition to splashing and the transition to the Leidenfrost state.

2. Experimental set-up

Figure 1 shows the schematics of the experimental set-up that allows us to observe and distinguish the different regimes of the droplets impacting the heated surfaces. We let ethanol droplets (density $\rho = 789$ kg m^{-3}, surface tension $\sigma = 22$ mN m^{-1}, viscosity $\mu = 1.1$ mPa s and boiling temperature $T_b = 78\,^{\circ}$C) fall on a polished sapphire plate (Goodfellow Cambridge Ltd) from a height h. By adjusting h, the velocity U of the droplet immediately before impacting the surface can be varied between 0.5 and 5 m s^{-1}. The droplets are generated by gently pushing the liquid out of a syringe with a syringe pump (PHD 22/2000, Harvard Apparatus), through a tube to a flat-tip, stainless steel needle (19 gauge, Hamilton Co.). The droplet forms at the tip of the needle and detaches when its weight overcomes the surface tension at the needle's tip. The pump is set at a sufficiently low flow rate (0.05 ml min^{-1}) to ensure that the droplet detachment is only due to gravity. As a result, all the droplets in our study have a uniform diameter $D = 2.5 \pm 0.1$ mm.

The sapphire plate is heated by placing it on a brass holder (see figure 1 for the schematics), which radially embeds six cartridge heaters and a temperature probe (Omega Inc.). The surface temperature T of the sapphire plate can be varied between room temperature and 500 °C and is measured independently with a surface temperature probe (N-141K, Anritsu) for each experiment. The brass holder has a hole in the centre that, together with the transparent sapphire plate, allows for bottom-view recordings of the impacting droplets.

To study the impact behaviours of droplets, we use two high-speed cameras (Fastcam SA1.1 & SA-X, Photron) to make synchronized recordings of the impact events from the side and the bottom. From the side-view recordings, the droplet diameter D and velocity U immediately before impact are measured. To obtain interferometric recordings of the impact from the bottom, we use a continuous wave laser (iFlex-Gemini, Qioptic) as illuminating light (see figure 1). As long as the liquid is separated from the sapphire surface by a small distance, light reflected from the top surface of the sapphire plate and from the bottom surface of the droplet causes interference patterns, which consist of dark and bright fringes, that can be recorded by the high-speed camera via a half-mirror and a microscope of long working distance. In contrast, the area over which the liquid touches the surface appears dark in the recordings, because most of the light escapes through the liquid/solid interface. Based on this distinct difference, we can identify, without ambiguity, whether an impacting droplet is in the film boiling regime, in the contact boiling regime or in a transitional regime. Thus, the interferometric recording offers a unique tool to accurately determine the temperature T_L beyond which the impact is in the Leidenfrost regime, i.e. the droplet makes no contact with the plate during the entire impact (Tran *et al.* 2012).

3. Experimental observations

We investigate the droplet behaviour while varying two control parameters: the surface temperature ($20\,^{\circ}\mathrm{C} \leqslant T \leqslant 500\,^{\circ}\mathrm{C}$) and the impact velocity ($0.5\ \mathrm{m\ s^{-1}} \leqslant U \leqslant 5.0\ \mathrm{m\ s^{-1}}$). The impact velocity is expressed in dimensionless form as Weber number $We = \rho D U^2/\sigma$ ($100 \leqslant We \leqslant 1500$), which measures the kinetic energy of the droplet in comparison to its surface energy. For fixed temperature, there is a critical Weber number We_C beyond which the impacting droplet makes a splash, i.e. disintegrates into smaller droplets during the spreading phase (Levin & Hobbs 1971; Mundo *et al.* 1995; Xu *et al.* 2005; Palacios *et al.* 2013; Riboux & Gordillo 2014). On the other hand, for each Weber number there is also a corresponding Leidenfrost temperature T_L. Hence, these two transitions naturally impose four typical behaviours of the impacting droplets in the *We*–*T* phase space: contact and no splashing (deposition regime), contact and splashing (contact–splash regime), neither contact nor splashing (bounce regime) and finally no contact, but splashing (film–splash regime).

In the deposition regime, in which the temperature and the Weber number are relatively low, the impacting droplets are deposited on the surface and boiled at the same time, as exemplified in figure 2(*a*). In this regime, the formation of vapour bubbles is clearly seen from the bottom view – the bubbles create dry patches on the surface which appear brighter in the bottom view, as opposed to the wetted areas that appear darker. The ejection of small droplets seen from the side view is clearly a result of the bursting of the vapour bubbles next to the surface. All the impacts in this regime are shown as (blue) diamonds in the *We*–*T* phase diagram (figure 3).

When increasing the Weber number, while keeping the temperature under T_L, the behaviour of impacting droplets undergoes a transition to the contact–splash regime in which either a liquid sheet or smaller droplets are ejected from the lamella as a result of the high liquid inertia during the spreading phase of the impact. Note that there are two different mechanisms for the ejection of secondary droplets from the main droplet. One mechanism is associated with the impact itself (defined as splashing), while the other is connected with the boiling process at the liquid/solid interface (contact boiling). The former happens at the very early stage of impact

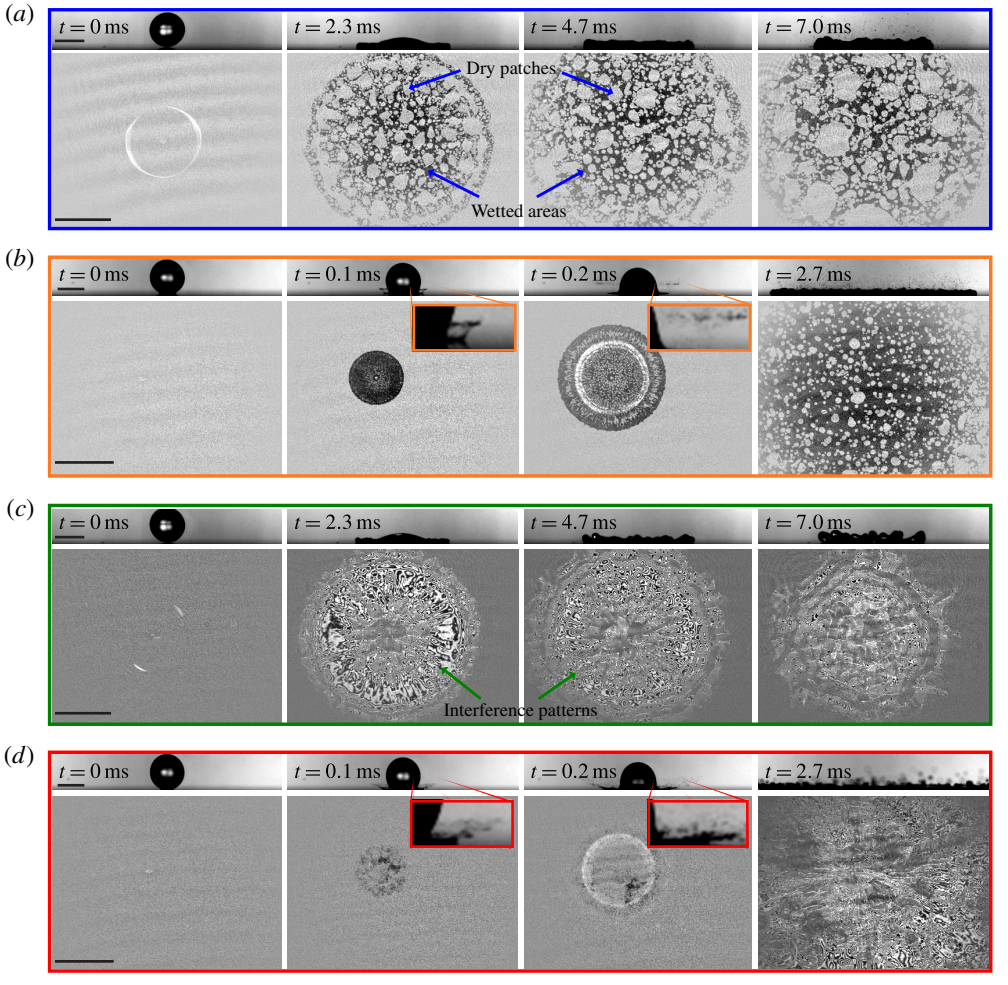

FIGURE 2. Typical sequences of ethanol droplets with diameter $D = 2.5$ mm impacting a sapphire plate for varying Weber number We and surface temperature T. All sequences have synchronized side-view and interferometric bottom-view recordings; the scale bars indicate 2 mm. (*a*) Deposition is observed for $We = 86$ and $T = 150\,^{\circ}\mathrm{C}$. Dark areas in the bottom view indicate contact, as does the spray of small droplets due to boiling at the solid/liquid interface in the side view. (*b*) For the same temperature but a higher impact velocity ($We = 1156$) the droplet makes a contact–splash. (*c*) At low impact velocity ($We = 85$) and higher temperature ($T = 200\,^{\circ}\mathrm{C}$) the droplet bounces off the surface. The interference pattern in the bottom view indicates that there is a lasting vapour film under the droplet during impact. (*d*) Now for the same temperature, but with high impact velocity ($We = 1190$), a film–splash is observed.

(e.g. at 0.1 ms in figure 2*b*) and originates from the expanding lamella, whereas the latter happens at a much later time (e.g. at 2.7 ms in figure 2*b*) and originates upwards from the middle of the liquid puddle, due to bursting of vapour bubbles at the solid/liquid interface. We are thereby able to accurately distinguish the impacts in the contact–splash regime from those in the deposition regime. All of the impacts in the contact–splash regime are collected and shown as orange squares in figure 3.

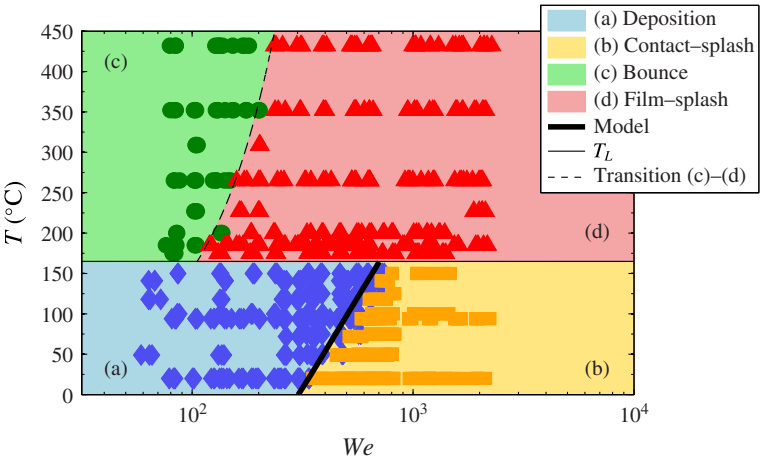

FIGURE 3. Phase diagram of the outcome of the impact of an ethanol droplet on a sapphire plate with varying surface temperature and Weber number. Four regimes are identified from the high-speed recordings: deposition (blue diamonds), bounce (green circles), contact–splash (orange squares) and film–splash (red triangles). The thin solid line indicates the dynamic Leidenfrost temperature T_L, the dashed line is a guide to the eye for the transition Weber number We_C between regimes (c) and (d) and the thick solid line indicates the transition Weber number between regimes (a) and (b) as predicted by the model explained in § 4.

Once the surface temperature is above the Leidenfrost temperature, the droplet and the surface are separated by a thin vapour film during the entire impact time. At a small Weber number, an impacting droplet spreads and rebounds from the surface as if the surface were superhydrophobic. Figure 2(*c*) shows such a bouncing droplet for $T = 200\,^{\circ}\mathrm{C}$ and $We = 85$. From the bottom view it is evident that there is no contact between the droplet and surface, as an interference pattern is observed for the entire impact duration, indicating a lasting vapour film. This regime is referred to as the bounce regime and is shown with (green) circles in figure 3.

With increasing impact velocity, while still keeping the surface temperature above T_L, the impact behaviour undergoes a transition to the film–splash regime. Figure 2(*d*) shows a series of representative images of an impacting droplet in this regime. Side-view measurements show that the droplet makes a splash at 0.1 ms. The interference pattern observed in the bottom-view recording during the entire impact process indicates that there is indeed a vapour film that separates the liquid and the surface. In the phase diagram shown in figure 3, this regime corresponds to the region with red triangles.

By identifying the characteristic behaviours of all experiments, out of the *We*–*T* parameter space we obtain the phase diagram for impacting ethanol droplets on a sapphire plate. The four well-separated regions correspond to the four aforementioned behaviours. Notably, the Leidenfrost transition marked by a dashed line, which separates the contact boiling regimes (deposition and contact–splash) and the film boiling regimes (bounce and film–splash), shows little dependence on the Weber number and can be approximated as $T_L \approx 165\,^{\circ}\mathrm{C}$. This result is consistent with the value of T_L for ethanol on a smooth aluminium surface that was reported previously by Wang *et al.* (2000). Note that the insensitive dependence of T_L on *We* found here

is not inconsistent with the recently found, stronger dependence of T_L on We for water (Tran *et al.* 2012), because of the difference both in the working liquid and in the ranges of Weber number investigated: in our present study, the Weber number ranges from 100 to 1500, whereas in Tran *et al.* (2012), it ranged from 0.5 to 600. Nevertheless, this insensitivity of T_L on We in the case of ethanol on sapphire is intriguing and deserves further studies for other combinations of materials.

In contrast to the, at most, weak dependence of T_L on We, the critical Weber number We_C, at which the transition to splashing occurs, is a strongly non-monotonic function of T. In the contact boiling regime, the transition to splashing separates the deposition regime from the contact–splash regime. The transition starts at $T = 20\,^{\circ}\mathrm{C}$ and $We_C = 350$, which agrees with the previously reported value of the transition to splashing of ethanol droplets impacting a smooth surface at room temperature (Palacios *et al.* 2013). As the temperature increases, We_C also increases until it reaches $We = 850$ at a temperature close to T_L. This is striking because it shows that splashing is considerably suppressed (from $We_C = 350$ to $We_C = 850$) as the surface temperature increases, though both surface tension and viscosity decrease with increasing temperature.

As the surface temperature is increased beyond T_L, We_C suddenly drops to a very small value $We_C = 110$ and only increases weakly to $We_C = 200$ when the surface temperature reaches $T = 450\,^{\circ}\mathrm{C}$ in this regime. Thus, the transition to splashing is not only discontinuous at T_L but also exhibits distinctively different behaviours in the film boiling and the contact boiling regimes.

To the best of our knowledge, the splash transition of a drop on a heated plate below T_L has not been reported previously, but the splash transition in the Leidenfrost state was reported by Wachters & Westerling (1966) ($We_C = 80$ for various liquids) and by Biance, Pirat & Ybert (2011) ($We_C = 300$–360, various liquids). Although all studies show a weak temperature dependence, the results differ, so clearly the Weber number and plate temperature are not the only relevant control parameters for splashing in the film boiling regime.

4. Modelling the contact–splash transition

To explain the experimental observations in the preceding section, we make use of the theory by Riboux & Gordillo (2014, 2015). The first step of this theory to describe the disintegration of the droplet during the initial phase after impact is to determine the ejection time t_e, i.e. the instant at which the lamella is first ejected. This time follows from the momentum balance (Riboux & Gordillo 2014, equation (1))

$$c_1 Re^{-1} t_e^{-1/2} + Re^{-2} Oh^{-2} = c^2 t_e^{3/2}, \tag{4.1}$$

with the Reynolds number $Re = \rho U R/\mu$, the Ohnesorge number $Oh = \mu/\sqrt{\rho R \sigma}$ and the drop radius $R = D/2$. The constants $c_1 \simeq \sqrt{3}/2$ and $c^2 = 1.2$ are adjusted to describe the experiments of Riboux & Gordillo (2014). Once t_e is calculated, the initial thickness of the edge of the lamella and its initial tangential velocity are determined as $h_t(t_e) \propto t_e^{3/2}$ and $v_t(t_e) \propto t_e^{-1/2}$, respectively (Riboux & Gordillo 2014). Here, the lower case variables indicate the dimensionless quantities constructed using R, U and R/U as the characteristic scales of length, velocity and time.

For times larger than t_e, the edge of the lamella experiences a vertical lift force F_L per unit length given by the addition of the classical aerodynamic lift force and the

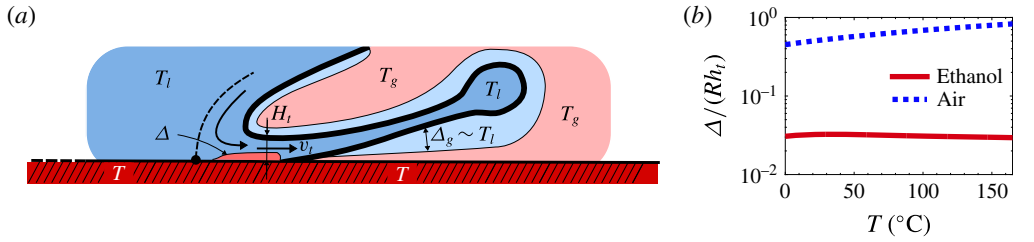

FIGURE 4. (*a*) Sketch of the lamella for an instant of time larger than t_e, illustrating the different regions in the flow and the temperature field deduced from the thermal boundary layer thicknesses. In the figure, blue and red represent low and high temperatures, respectively. Before the ethanol drop touches the plate, the drop is at room temperature $T_l \approx 20\,^{\circ}\mathrm{C}$, while the surrounding air is at $20\,^{\circ}\mathrm{C} \leqslant T_g \leqslant T$. After impact, a small spatial region in the liquid heats up to a temperature T and part of the gas surrounding the drop cools down to T_l. The widths of the regions where the liquid is heated up and the gas is cooled down are characterized by the thicknesses of their respective thermal boundary layers Δ and Δ_g. (*b*) Relative widths of the liquid and gas thermal boundary layers calculated using (4.4). The differences in the widths of the thermal boundary layers depicted in this figure are caused by the disparate values of the Prandtl numbers, $Pr \gtrsim 10$ for ethanol and $Pr_g(T) \simeq 0.7$ for air.

projection in the vertical direction of the lubrication force exerted by the gas beneath the lamella (Riboux & Gordillo 2014, equation (2)),

$$F_L = K_u \rho_g U^2 R v_t^2(t_e) h_t(t_e) + K_l \mu_g U v_t(t_e), \tag{4.2}$$

where the subscript g represents gas quantities, $K_u \simeq 0.3$ is a constant determined numerically and K_l depends logarithmically on the ratio $\lambda/(Rh_t)$, with λ the mean free path of gas molecules. In Riboux & Gordillo (2014) it is found that the critical lift force, above which the droplet disintegrates into smaller droplets, is given by

$$\left(\frac{F_L}{2\sigma}\right)^{1/2} = 0.14, \tag{4.3}$$

from which the critical impact velocity or, equivalently, We_C is calculated using (4.2) (see Riboux & Gordillo (2014) for details).

In order to make use of the splash criterion given by (4.3) and check whether the experimental observations in § 3 can be explained using the framework developed in Riboux & Gordillo (2014), it is mandatory to use the correct temperature-dependent physical properties of the two fluids involved in the splashing process. Before the drop touches the substrate, the liquid is at room temperature $T_l \approx 20\,^{\circ}\mathrm{C}$ and the gas temperature is $20\,^{\circ}\mathrm{C} \leqslant T_g \leqslant T$. However, as soon as the drop impacts the substrate, the liquid heats up and the gas cools down in the regions characterized by their respective thermal boundary layer thicknesses, Δ and Δ_g (sketched in figure 4*a*). To estimate both thicknesses, note first that the liquid particles feeding the lamella come from the region located to the right of the dashed line sketched in figure 4(*a*), which ends at the relative stagnation point present in the flow when the velocity field is described in a frame of reference moving at the wetting velocity $\sqrt{3/t}/2$ (Riboux & Gordillo 2014, 2015). Since the relative stagnation point is located at a distance from the root of the lamella proportional to its thickness, $Rh_t \propto Rt^{3/2}$, and the liquid

velocity feeding the liquid sheet is $Uv_t \propto Ut^{-1/2}$, the characteristic residence time of the fluid particles entering the lamella is $Rh_t(t_e)/(Uv_t(t_e))$, which coincides with the characteristic residence time of the gas particles flowing around the edge of the liquid sheet (Riboux & Gordillo 2014, 2015). Therefore, the ratios of the thicknesses of the thermal boundary layers and the thickness of the lamella at the ejection instant, $Rh_t(t_e)$, are given by

$$\frac{\Delta}{Rh_t} \propto \sqrt{\frac{\nu(T)}{RUh_t v_t Pr(T)}} \quad \text{and} \quad \frac{\Delta_g}{Rh_t} \propto \sqrt{\frac{\nu_g(T)}{RUh_t v_t Pr_g(T)}}, \tag{4.4a,b}$$

with $Pr(T)$ and $Pr_g(T)$ the temperature-dependent values of the Prandtl numbers for ethanol and air, respectively. Figure 4(*b*), where the ratios in (4.4) are represented, reveals that just a small region of the ethanol droplet in contact with the wall heats up to the temperature T and, therefore, most of the liquid flowing into the lamella is at room temperature. The width of the gas thermal boundary layer is, however, comparable to the width of the liquid sheet, as is sketched in figure 4(*a*). Consequently, most of the air located in between the lamella and the wall cools down to the temperature of the liquid, with the exception of the region closest to the substrate, where the air keeps its initial temperature T.

Taking this all into consideration, the term representing the viscous deceleration of the tip of the lamella in the momentum balance (4.1) is calculated using the following expression for the liquid viscosity:

$$\mu(T) = \exp\left(\sum_{i=0}^{5} a_i T^i\right) \times 10^{-3} \text{ Pa s} \tag{4.5}$$

with $a_0 = 5.8942 \times 10^{-1}$, $a_1 = -2.2540 \times 10^{-2}$, $a_2 = 1.0283 \times 10^{-4}$, $a_3 = -8.8574 \times 10^{-7}$, $a_4 = 4.7884 \times 10^{-9}$, $a_5 = -9.7493 \times 10^{-12}$ and T in degrees Celsius (Vargaftik 1975). Because most of the liquid feeding the lamella keeps its initial temperature, the liquid density and the interfacial tension coefficient in (4.1) and (4.3) are evaluated at room temperature. The expressions for the air density and the mean free path of gas molecules in (4.2) depend on the wall temperature as $\rho_g = 10^5/(287 \times T)$ kg m^{-3} and $\lambda = 68 \times 10^{-9} \times T/293$ m, with the temperature in kelvin. However, since the gas located beneath the lamella cools down to the ethanol temperature, the value of the gas viscosity in (4.2) is evaluated at room temperature, $\mu_g = 1.86 \times 10^{-5}$ Pa s. We now employ (4.3) using the expressions for the physical properties of both the ethanol and the air as detailed above, finding that the calculated critical velocity for splashing is in quantitative agreement with experiments, as figure 3 shows.

Recent work by Liu, Tan & Xu (2015) shows that when the thickness of the lamella is equal to the fastest growing wavelength of a Kelvin—Helmholtz type instability, a droplet will splash. As this model does not give a prediction based on the impact parameters of either the lamella thickness or the fastest growing wavelength, we cannot use this model to predict the critical Weber number for our experiments. With the somewhat older, but very similar model by Xu *et al.* (2005) we were able to fit a splash threshold to our experiments. However, the fitting parameter reported by Xu *et al.* (2005), a universal 0.45, is not in accord with our experiments. The best fit of that model to our data is with a fitting parameter of 0.8, including the experiments at room temperature.

5. Conclusions

In conclusion, we have investigated the splashing and Leidenfrost transitions for ethanol droplets impacting a temperature-controlled sapphire plate. We have identified four different regimes in the explored *We*–*T* phase space: deposition, contact–splash, bounce and film–splash. While the dynamic Leidenfrost transition temperature T_L shows little dependence on *We*, the transition to splashing shows a strong and non-monotonic dependence on *T*. By incorporating the temperature dependence of the physical properties in the theory by Riboux & Gordillo (2014, 2015), we can quantitatively explain the splashing transition for surface temperatures below T_L. The splashing transition for droplets in the Leidenfrost state remains the subject of future research.

Acknowledgements

This study was financially supported by a European Research Council (ERC) advanced grant and the Spanish MINECO under Project DPI2014-59292-C3-2-P, partly financed through European funds.

References

Bernardin, J. D., Stebbins, C. J. & Mudawar, I. 1997 Mapping of impact and heat transfer regimes of water drops impinging on a polished surface. *Intl J. Heat Mass Transfer* **40** (2), 247–267.

Biance, A. L., Pirat, C. & Ybert, C. 2011 Drop fragmentation due to hole formation during Leidenfrost impact. *Phys. Fluids* **23**, 022104.

Bouwhuis, W., van der Veen, R. C. A., Tran, T., Keij, D. L., Winkels, K. G., Peters, I. R., van der Meer, D., Sun, C., Snoeijer, J. H. & Lohse, D. 2012 Maximal air bubble entrainment at liquid-drop impact. *Phys. Rev. Lett.* **109** (26), 264501.

Chandra, S. & Avedisian, C. T. 1991 On the collision of a droplet with a solid surface. *Proc. R. Soc. Lond.* A **432**, 13–41.

Driscoll, M. M., Stevens, C. S. & Nagel, S. R. 2010 Thin film formation during splashing of viscous liquids. *Phys. Rev.* E **82** (3), 036302.

Inada, S., Miyasaka, Y., Sakamoto, K. & Hojo, K. 1988 Liquid–solid contact state and fluctuation of the vapor film thickness of a drop impinging on a heated surface. *J. Chem. Engng Japan* **21** (5), 463–468.

Khavari, M., Sun, C., Lohse, D. & Tran, T. 2015 Fingering patterns during droplet impact on heated surfaces. *Soft Matt.* **11** (17), 3298–3303.

Kolinski, J., Rubinstein, S., Mandre, S., Brenner, M. P., Weitz, D. & Mahadevan, L. 2012 Skating on a film of air: drops impacting on a surface. *Phys. Rev. Lett.* **108** (7), 074503.

Latka, A., Strandburg-Peshkin, A., Driscoll, M. M., Stevens, C. S. & Nagel, S. R. 2012 Creation of prompt and thin-sheet splashing by varying surface roughness or increasing air pressure. *Phys. Rev. Lett.* **109** (5), 054501.

Lembach, A. N., Tan, H. B., Roisman, I. V., Gambaryan-Roisman, T., Zhang, Y., Tropea, C. & Yarin, A. L. 2010 Drop impact, spreading, splashing, and penetration into electrospun nanofiber mats. *Langmuir* **26** (12), 9516–9523.

Levin, Z. & Hobbs, P. V. 1971 Splashing of water drops on solid and wetted surfaces: hydrodynamics and charge separation. *Phil. Trans.* A **269**, 555–585.

Liu, Y., Tan, P. & Xu, L. 2015 Kelvin–Helmholtz instability in an ultrathin air film causes drop splashing on smooth surfaces. *Proc. Natl Acad. Sci. USA* **112** (11), 3280–3284.

Mandre, S. & Brenner, M. P. 2011 The mechanism of a splash on a dry solid surface. *J. Fluid Mech.* **690**, 148–172.

MANDRE, S., MANI, M. & BRENNER, M. P. 2009 Precursors to splashing of liquid droplets on a solid surface. *Phys. Rev. Lett.* **102** (13), 134502.

MANI, M., MANDRE, S. & BRENNER, M. P. 2010 Events before droplet splashing on a solid surface. *J. Fluid Mech.* **647**, 163–185.

MUNDO, C., SOMMERFELD, M. & TROPEA, C. 1995 Droplet-wall collisions: experimental studies of the deformation and breakup process. *Intl J. Multiphase Flow* **21** (2), 151–173.

NAIR, H., STAAT, H. J. J., TRAN, T., VAN HOUSELT, A., PROSPERETTI, A., LOHSE, D. & SUN, C. 2014 The Leidenfrost temperature increase for impacting droplets on carbon-nanofiber surfaces. *Soft Matt.* **10** (13), 2102–2109.

PALACIOS, J., HERNÁNDEZ, J., GÓMEZ, P., ZANZI, C. & LÓPEZ, J. 2013 Experimental study of splashing patterns and the splashing/deposition threshold in drop impacts onto dry smooth solid surfaces. *Exp. Therm. Fluid Sci.* **44**, 571–582.

QUÉRÉ, D. 2013 Leidenfrost dynamics. *Annu. Rev. Fluid Mech.* **45** (1), 197–215.

REIN, M. 1993 Phenomena of liquid-drop impact on solid and liquid surfaces. *Fluid Dyn. Res.* **12** (2), 61–93.

RIBOUX, G. & GORDILLO, J. M. 2014 Experiments of drops impacting a smooth solid surface: a model of the critical impact speed for drop splashing. *Phys. Rev. Lett.* **113** (2), 024507.

RIBOUX, G. & GORDILLO, J. M. 2015 The diameters and velocities of the droplets ejected after splashing. *J. Fluid Mech.* **772**, 630–648.

ROISMAN, I. V., RIOBOO, R. & TROPEA, C. 2002 Normal impact of a liquid drop on a dry surface: model for spreading and receding. *Proc. R. Soc. Lond.* A **458** (2022), 1411–1430.

SHIROTA, M., VAN LIMBEEK, M. A. J., SUN, C., PROSPERETTI, A. & LOHSE, D. 2015. Dynamic Leidenfrost temperature for droplet impact on an isothermal superheated surface (submitted).

SINHA-RAY, S., ZHANG, Y. & YARIN, A. L. 2011 Thorny devil nanotextured fibers: the way to cooling rates on the order of 1 kW cm^{-2}. *Langmuir* **27** (1), 215–226.

STEVENS, C. S. 2014 Scaling of the splash threshold for low-viscosity fluids. *Europhys. Lett.* **106** (2), 24001.

THORODDSEN, S. T. & SAKAKIBARA, J. 1998 Evolution of the fingering pattern of an impacting drop. *Phys. Fluids* **10** (6), 1359–1374.

TRAN, T., STAAT, H. J. J., PROSPERETTI, A., SUN, C. & LOHSE, D. 2012 Drop impact on superheated surfaces. *Phys. Rev. Lett.* **108** (3), 036101.

TRAN, T., STAAT, H. J. J., SUSARREY-ARCE, A., FOERTSCH, T. C., VAN HOUSELT, A., GARDENIERS, H. J. G. E., PROSPERETTI, A., LOHSE, D. & SUN, C. 2013 Droplet impact on superheated micro-structured surfaces. *Soft Matt.* **9** (12), 3272–3282.

TSAI, P., HENDRIX, M. H. W., DIJKSTRA, R. R. M., SHUI, L. & LOHSE, D. 2011 Microscopic structure influencing macroscopic splash at high Weber number. *Soft Matt.* **7** (24), 11325–11333.

VARGAFTIK, N. B. 1975 *Handbook of Physical Properties of Liquids and Gases*. Springer.

VAN DER VEEN, R. C. A., HENDRIX, M. H. W., TRAN, T., SUN, C., TSAI, P. A. & LOHSE, D. 2014 How microstructures affect air film dynamics prior to drop impact. *Soft Matt.* **10** (21), 3703–3707.

VISSER, C. W., FROMMHOLD, P. E., WILDEMAN, S., METTIN, R., LOHSE, D. & SUN, C. 2015 Dynamics of high-speed micro-drop impact: numerical simulations and experiments at frame-to-frame times below 100 ns. *Soft Matt.* **11** (9), 1708–1722.

VISSER, C. W., TAGAWA, Y., SUN, C. & LOHSE, D. 2012 Microdroplet impact at very high velocity. *Soft Matt.* **8** (41), 10732–10737.

WACHTERS, L. H. J. & WESTERLING, N. A. J. 1966 The heat transfer from a hot wall to impinging water drops in the spheroidal state. *Chem. Engng Sci.* **21**, 1047–1056.

WANG, A. B., LIN, C. H. & CHEN, C. C. 2000 The critical temperature of dry impact for tiny droplet impinging on a heated surface. *Phys. Fluids* **12**, 1622–1625.

WEICKGENANNT, C. M., ZHANG, Y., SINHA-RAY, S., ROISMAN, I. V., GAMBARYAN-ROISMAN, T., TROPEA, C. & YARIN, A. L. 2011 Thorny devil nanotextured fibers: the way to cooling rates on the order of 1 kW cm^{-2}. *Phys. Rev.* E **84** (3), 036310.

WORTHINGTON, A. M. 1876 On the forms assumed by drops of liquids falling vertically on a horizontal plate. *Proc. R. Soc. Lond.* **25** (171-178), 261–272.

XU, L., ZHANG, W. W. & NAGEL, S. R. 2005 Drop splashing on a dry smooth surface. *Phys. Rev. Lett.* **94** (18), 184505.

YAO, S. C. & CAI, K. Y. 1988 The dynamics and Leidenfrost temperature of drops impacting on a hot surface at small angles. *Exp. Therm. Fluid Sci.* **1** (4), 363–371.

YARIN, A. L. 2006 Drop impact dynamics: splashing, spreading, receding, bouncing.... *Annu. Rev. Fluid Mech.* **38**, 159–192.

YARIN, A. L. & WEISS, D. A. 1995 Impact of drops on solid surfaces: self-similar capillary waves, and splashing as a new type of kinematic discontinuity. *J. Fluid Mech.* **283** (1), 141–173.